High-Resolution Continuous-Wave-Diode Laser Cavity Ring-Down Spectroscopy of the Hydrogen Fluoride Dimer in a Pulsed Slit Jet Expansion: Two Components of the $N = 2$ Triad near 1.3 μm†

Michael Hippler,‡,§ Lars Oeltjen,‡ and Martin Quack*,‡

Physical Chemistry, ETH Zürich, CH-8093 Zürich, Switzerland, and Department of Chemistry, University of Sheffield, Sheffield S3 7HF, England

Received: August 28, 2007; In Final Form: October 16, 2007

The near-infrared overtone spectra of the prototypical hydrogen-bond hydrogen fluoride dimer $(HF)_2$ contain rich information on hydrogen bond dynamics. We report a study of the $N = 2$ triad involving excitations with two quanta of HF stretching in $(HF)_2$ around 1.3 μm (7500−7800 cm^{-1}) by means of continuous-wave-diode laser cavity ring-down spectroscopy in a pulsed supersonic slit jet expansion. The analysis of the rotationally resolved overtone spectra allows the study of vibrational mode-selective kinetics, such as hydrogen bond predissociation with lifetimes τ_{PD} and tunneling rearrangement (switching) processes with periods τ_{sw} obtained from the tunneling splitting $\Delta\tilde{\nu}_T$ in highly excited vibrational states. The $K_a = 1 \leftarrow 0$ transition of the $N_j = 2_2$ band of $(HF)_2$ has been reinvestigated by us in a supersonic jet expansion; the much improved data obtained here are in excellent agreement with several previous experimental results. Our analysis provides subband-level positions and properties $\tilde{\nu}_0(K_a = 1(A^+)) = 7711.37956(66)$ cm^{-1}, $\Delta\tilde{\nu}_T = 0.0936(10)$ cm^{-1}, and $\tau_{PD} = 1.3-1.9 \times 10^{-9}$ s, depending on the level symmetry A^+ and B^+. We have also analyzed spectra of the $N_j = 2_1$ band, which we have observed for the first time in a supersonic jet with rotational resolution. For the $K_a = 0 \leftarrow 0$ transition of this band, we find the band center at $\tilde{\nu}_0(A^+) = 7550.3555(26)$ cm^{-1} and a tunneling splitting of $\Delta\tilde{\nu}_T = 0.0150(37)$ cm^{-1}. This level involves mostly excitation of the H-bonded HF stretching with two quanta. The mode-selective tunneling switching is in agreement with a simple picture of inhibited tunneling. These experimental values are close to those calculated on the "SO-3" potential energy hypersurface of Klopper, Quack, and Suhm. The $N = 2$ triad also exhibits a strongly mode-selective predissociation dynamics, with a predissociation lifetime $\tau_{PD} = 4.99(84) \times 10^{-11}$ s in the $N_j = 2_1$ level, which is more than 20 times shorter than that for the $N_j = 2_2$ level.

1. Introduction

Molecular beam techniques have been crucial in new developments in high-resolution molecular spectroscopy, and Giacinto Scoles has been among the pioneers in developing and applying such techniques (see the extensive reviews in the two books edited by him[1] as well as refs 2 and 3, for example). Early molecular beam spectroscopy was restricted to sensitive molecular beam electric resonance[4] or laser-induced fluorescence detection techniques.[5−8] Our group has been involved in developing high-resolution supersonic jet Fourier transform infrared (FTIR) spectroscopy, which has the advantage of covering very broad spectral ranges, still often at the Doppler limit of supersonic jet spectra.[9−11] The lower sensitivity of this technique, however, restricts its application to strong absorptions, usually in the fundamental range. The sensitivity can be slightly improved by a combination with diode laser absorption spectroscopy of supersonic jets.[11−18] An alternative technique of higher sensitivity is the use of enclosive He-flow cooling instead of supersonic jets.[19]

An obvious new technique of high sensitivity is cavity ring-down (CRD) spectroscopy.[20−22] Originally this technique was introduced in combination with pulsed lasers, which somewhat limits its resolution. However, we and others have extended the technique to the use of continuous-wave (cw) lasers of very narrow band widths.[23−25] The use of these high-resolution cw-CRD methods with pulsed supersonic jets constitutes a problem, as the index of refraction within the cavity changes when the gas pulse arrives, and thus the resonance-matching condition for the cavity gets lost. We have recently overcome this difficulty by our development of cw-CRD spectroscopy in a pulsed supersonic slit jet expansion as a new tool for high-resolution and high-sensitivity molecular beam spectroscopy.[26,27] With rather broadly tunable near-infrared diode lasers of very narrow bandwidth (<1 MHz), this technique compares very favorably with other high-resolution methods for the study of weak absorptions.[28] For instance, we have provided a very precise measurement of the $\nu_2 + \nu_3$ ($J = 0$) level of the methane overtone icosad by this technique among other things.[27]

In the present investigation, we use this technique for addressing some difficult open questions in the weak overtone absorption spectrum of the hydrogen fluoride dimer $(HF)_2$. Hydrogen fluoride clusters are very simple, prototypical for hydrogen-bonded clusters in general, and are thus ideal for fundamental studies of hydrogen-bond dynamics.[29,30] Because of its small size, the dimer is also amenable to high-quality ab

† Part of the "Giacinto Scoles Festschrift".

* Corresponding author. Address: ETH Zürich, Laboratory of Physical Chemistry, Wolfgang-Pauli-Strasse 10, CH-8093 Zürich, Switzerland. Fax: +41 44 632 10 21. Phone: + 41 44 632 44 21. E-mail: Martin@Quack.ch.

‡ ETH Zürich.

§ University of Sheffield.

10.1021/jp076894s CCC: $37.00
Published on Web 11/20/2007

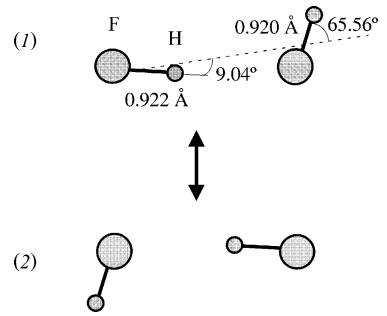

Figure 1. Equilibrium structure of $(HF)_2$ in the ground state (bond lengths and angles are taken from ref 37). The dashed line connects the centers of gravity of the HF subunits. In conformers (1) and (2), the HF subunits exchange their role as hydrogen-bond donor and acceptor. The potential barrier for this hydrogen-bond switching process is about 350 (hc) cm^{-1}.

initio calculations,[31] including the development of full-dimensional (6D) potential energy hypersurfaces,[29,32−37] variational grid techniques,[38−41] and 6D quantum Monte Carlo calculations of rovibrational energy levels.[32,42−44] The HF dimer has also been the subject of several detailed high-resolution spectroscopic investigations, for example, in the microwave,[4] far-infrared,[32,42,45,46] mid-infrared,[47,48] and near-infrared[49−51] spectral ranges. An accurate experimental determination of D_0 is noteworthy in relation to predissociation dynamics[52] and to the determination of D_e.[37,44] In this context, the extension to binding in the larger $(HF)_n$ clusters may also be mentioned.[53,54]

Particularly in the HF-stretching overtone absorptions of $(HF)_2$ and its isotopomers, there remain some important open questions, which we shall address here. These specifically concern the detailed influence of HF stretching excitation on the two processes of hydrogen-bond switching (Figure 1) and hydrogen-bond vibrational predissociation (eq 1):

$$(HF)_2^* \rightarrow 2HF \qquad (1)$$

Jet cooling in the present work greatly reduces the spectral congestion by hot-band transitions and also increases the spectral resolution by decreasing the Doppler width of rovibrational transitions. Insight into the vibrational mode-specific intramolecular dynamics of $(HF)_2$ can be derived, provided a detailed assignment and analysis is available (for example, of homogeneous rovibrational line widths and tunneling splittings, which contain information about predissociation processes and hydrogen-bond switching, respectively).

Vibrational bands of HF dimer, which are characterized by the same total number of HF-stretching quanta, have nearly the same energy and are grouped together to a polyad system. In the polyad nomenclature, N_j denotes the vibrational band component j within the polyad N; N refers to the total number of stretching quanta distributed among the two HF monomer subunits of the dimer, and the index j orders the components with increasing energy. The $N = 2$ polyad (corresponding to the first HF stretching overtone) is particularly interesting for studying mode-specific dynamics in the HF dimer, since it has three different possibilities for distribution of the HF stretching quanta among the HF subunits. In $N_j = 2_2$, the vibrational excitation is approximately localized in the hydrogen-bond acceptor HF corresponding to excitation with two quanta of the "free" HF stretching, and, in $N_j = 2_1$, it is localized in the hydrogen-bond donor HF corresponding to excitation with two quanta of the "H-bonded" HF stretching. In $N_j = 2_3$, both HF subunits are excited by one quantum. We prefer, in this paper, the polyad notation of ref 51 over the local mode notation, which is also frequently used. The advantage of the polyad notation is its greater generality as labels for the true eigenstates (the local mode assignments are only *approximate* and thus not fully correct). The advantage of the local mode notation is its insight into the approximate nature of the excitation. Strictly speaking, however, the real local mode states do not correspond to the observed spectroscopic eigenstates. Nevertheless, if one uses the local mode labels as approximate labels for the eigenstates, one has the following correlation: $|2_1\rangle$: $|(v_b = 2, v_f = 0)\rangle$; $|2_2\rangle$: $|(v_b = 0, v_f = 2)\rangle$; and $|2_3\rangle$: $|(v_b = 1, v_f = 1)\rangle$.

In this investigation, we present the first experimental observation of the polyad component $N_j = 2_1$ in a supersonic jet expansion, and we provide an assignment and analysis to obtain level parameters for this component. The assignment is corroborated by ab initio calculations. The predissociation and hydrogen bond switching dynamics in $N_j = 2_1$ is compared with the corresponding dynamics in the polyad component $N_j = 2_2$, which demonstrates the interaction of HF stretching modes with various dynamic processes.

2. Experimental

cw-CRD spectroscopy in pulsed supersonic jets has been used to obtain high-resolution spectra of the first HF stretching overtone of $(HF)_2$. Only a brief account of this technique will be given here, since it is described in more detail in refs 23, 26, and 27. In single-frequency mode, the tunable external cavity InGaAsP laser diode (Radians Innova) emits a beam of a few milliwatts between 7465 and 8025 cm^{-1}. The instrumental bandwidth of about 1 MHz provides a resolving power of more than 2×10^8. Part of the beam is used for an external monitor (500 MHz) étalon. The main part passes through an acousto-optical modulator (Isomet 1205C-2), where the first-order deflection is coupled into a single-mode optical fiber. A few hundred microwatts of power are coupled into the ring-down cavity employing a lens to match the geometry of the laser beam to the single transversal cavity mode TEM_{00}. The cavity consists of two concave mirrors of high reflectivity R (Newport SuperMirrors, $R \geq 99.97\%$, radius 1 m) separated by 32 cm. The cavity is contained within a vacuum chamber. The 33 mm $\times$ 0.1 mm slit of a pulsed solenoid valve is placed at a distance of 5 mm and aligned along the optical axis of the cavity. The home-built pulsed valve[26,27,55,56] is made of stainless steel to be corrosion resistant. It produces gas pulses of about 1.2 ms duration, which generate a background pressure in the vacuum chamber below 5×10^{-3} mbar at a stagnation pressure of 250 mbar and a repetition rate of 10 Hz. The pumping system consists of an 8000 L/s oil diffusion pump backed by a combination of a roots pump and a mechanical roughing pump. Each mirror is contained in a small compartment made of Teflon foil and flushed continuously with a small flow of helium. In this way, the mirrors are protected from HF and oil vapor exposure, and no performance degradation is noticed during several months of operation.

Mode matching of the cavity length to the laser wavelength is achieved by a passive scheme, where the cavity length is periodically modulated at 20 Hz by slightly more than one free spectral range employing a piezoelectric transducer mounted to one of the cavity mirrors.[26,27] The cavity is thus twice in resonance with the laser wavelength during one period. Since the modulation is periodic, the occurrence of the first resonance during one period can be used to predict the first resonance in the following period. At a given delay before the predicted resonance event, the solenoid valve is activated. If the resonance occurs during a 300 μs window within the maximum of the

gas pulse, the acousto-optical modulator is switched-off and data acquisition is triggered. A fast InGaAs photodetector (NewFocus, 125 MHz) then detects the exponential decay of the transmitted intensity after the cavity and stores the decay curve in a digital oscilloscope (Tektronix TDS 220, bandwidth reduced to 20 MHz). Several decay curves are averaged in the oscilloscope and then transferred to a computer for an analysis. From a fit of the exponential decaying intensity to $I(t) = x + I_0 \exp(-kt)$, the ring-down constant k is obtained, which is essentially given by αc and an additional spectral baseline.[23,26,27]

$$I(t) = x + I_0 \exp(-kt) \tag{2}$$

$$k = \alpha c + (1 - R)c/l \tag{3}$$

c is the speed of light, and the absorption coefficient α of the absorbing species inside the cavity is related to the absorption cross-section $\sigma = \alpha/C$, where C is the particle density. More generally one has

$$\alpha = \sigma \int_0^l C'(z)\mathrm{d}z \tag{4}$$

where the integration is extended over the range of nonnegligible concentration $C'(z)$ in the supersonic jet expansion. Typical decay times $\tau = 1/k$ for the empty cavity are 8 μs. Since light is typically reflected back and forth several thousand times in the cavity during the time for the measured decay signals, effective absorption path lengths of several kilometers are obtained, which explains the extraordinary sensitivity of CRD spectroscopy. In jet measurements, concentrations are not uniform and, in general, not known, and the absorbance per pass $A_{pp} = \alpha l$ is then an appropriate quantity, where l is the distance between the two mirrors. Resonances, which occur without the nozzle operating, are not wasted in our scheme. They are stored in a second oscilloscope and analyzed to obtain the baseline during the same spectral scan.

A CRD absorption spectrum is obtained by scanning the laser frequency and recording signal and background. The resulting spectra are linearized using the fringes of a 500 MHz étalon and calibrated to absolute frequency by spectroscopic reference lines. For the $N_j = 2_1$ band, we used H_2O transitions[57] recorded by CRD spectroscopy of about 10 mbar of air at room temperature for calibration, and for the $N_j = 2_2$ band, the HF monomer first overtone transition $P(1)$ at 7709.68249 cm^{-1} as a reference line obtained from ref 18 was recorded simultaneously in a 10 cm absorption cell with about 10 mbar of HF at room temperature. The calibrated spectra have an estimated absolute wavenumber or repetency[58] accuracy of about 0.001 cm^{-1}.

After extensive test trials, a mixture of 4% HF (PanGas, ≥99.9%), 9% N_2O (PanGas, ≥99.5%), and 87% Ar (PanGas, ≥99.998%) was identified to yield maximum dimer concentrations under the present experimental jet conditions. Ar as a seeding gas enhances jet cooling during the supersonic expansion. N_2O is added to the Ar−HF mixture since it promotes dimer formation compared to a pure Ar−HF mixture.[18,59] Gas handling is a crucial point of the experiment since HF is highly corrosive, especially in the presence of water. Thus, great care has to be taken to avoid humidity in the system. The components of the gas-handling system and of the pulsed valve have to be highly corrosion resistant and are thus made of stainless steel or Monel, a nickel−copper alloy. Baratron absolute capacitance manometers are employed for pressure measurements in the gas handling system. After its use in the expansion, the gas mixture passes through an absorber containing dried soda lime (Na_2CO_3) to remove HF. We draw attention to the potentially dangerous properties of hydrogen fluoride in terms of its physiological effects, which requires appropriate accident prevention, although, in working for several decades with this compound, we never actually experienced an accident.

3. Methods for Analysis

3.1. Rotational Analysis of the $(HF)_2$ Spectra. Figure 1 shows the equilibrium structure of $(HF)_2$ in its ground state. In the two equivalent conformers (1) and (2), the HF molecules exchange their roles as hydrogen-bond donors and acceptors. The planar conformers belong to the point group C_S. However, both conformers easily interconvert by a tunneling process ("hydrogen-bond switching"). The molecular symmetry group M_{S4} used to describe $(HF)_2$ is thus the direct product of the space inversion group and the permutation group corresponding to the interchange of the two HF units. The symmetry with respect to space inversion is indicated by the parity label "+" (symmetric) or "−" (antisymmetric). The symmetry with respect to permutation is indicated by A (symmetric) or B (antisymmetric). One has thus a total of 4 species A^+, A^-, B^+, and B^-. Each A' level in C_s symmetry (such as the vibrational ground state or the vibrationally excited states investigated here) is split by tunneling in an A^+/B^+ pair in the M_{S4} group, and each A'' level in an A^-/B^- pair (we use the systematic notation of ref 60, explicitly indicating the parity (±) as a superscript in the species symbol).[45,58,60] We denote the tunneling-vibrational symmetry species as Γ_{vt}. The rotational species Γ_r has to be included to derive the total symmetry species $\Gamma_{vtr} = \Gamma_{vt}\Gamma_r$, which finally describes the symmetry of rovibrational levels of $(HF)_2$. The electric dipole selection rules require a change of parity during a radiative transition

$$+ \leftrightarrow - \tag{5}$$

and conservation of nuclear spin symmetry

$$A \not\leftrightarrow B \tag{6}$$

The simulation of rovibrational spectra of $(HF)_2$ takes advantage of the fact that it is a nearly symmetric top molecule with asymmetry parameter $\kappa = -0.9998$.[4,45−51] Subbands have either parallel or perpendicular character with respect to the near symmetry axis "A", which corresponds to the F−H···F axis of the molecule. Experimental spectra can be fit to a truncated power series expansion in $J(J + 1)$ (eq 7),

$$\frac{E_{K_a}(J)}{hc} = \tilde{\nu}_{K_a} + \left(\bar{B}_{K_a} \pm \frac{1}{4}\,\delta_{K_a1} b_{K_a}\right)J(J + 1) - [D_{K_a} \mp (\delta_{K_a1} + \delta_{K_a2})d_{K_a}]J^2(J + 1)^2 + [H_{K_a} \pm (\delta_{K_a2} + \delta_{K_a3})h_{K_a}]J^3(J + 1)^3 \tag{7}$$

which reproduces the rovibronic energy level structure of $(HF)_2$ with good accuracy.[46] $\tilde{\nu}_{K_a}$ is the nominal subband center for a given K_a level of a vibrational-tunneling state extrapolated to $J = 0$, $\bar{B}_{K_a} = (B_{K_a} + C_{K_a})/2$ denotes the average rotational constant of a nearly symmetric top, asymmetry splitting terms are given by $b_{K_a} = (B_{K_a} - C_{K_a})/2$, d_{K_a} and h_{K_a}, centrifugal distortion constants are given by D_{K_a} and H_{K_a}, and $\delta_{K_ai} (i = 1,2,3)$ is the Kronecker delta.[42,46] The upper signs in this equation apply to levels with $K_a + K_c = J$, the lower ones apply to $K_a + K_c = J + 1$. Ground-state spectroscopic parameters employed in the fit are taken from refs 42, 46, and 61 and are held fixed during the fitting process.

Relative line intensities in a subband are approximated by symmetric top Hönl−London formulae.[62] Appropriate nuclear spin statistical weights have to be applied, since the nuclear spin statistics is responsible for an intensity alternation of even and odd *J*-values within a branch. The values of the nuclear-spin statistical weights are $g_A = 10$ for the symmetric (*A*) nuclear spin wave function combining with the symmetric (*A*) motional wave function, and $g_B = 6$ for the antisymmetric (*B*) nuclear spin function combining with the antisymmetric (*B*) motional wave function.[42,45]

The conformers (1) and (2) in Figure 1 correspond to time-dependent states that interchange with a characteristic tunneling period[30,63,64]

$$\tau_{sw} = \frac{h}{\Delta E_{sw}} = \frac{1}{c|\Delta\tilde{\nu}_{sw}|} \tag{8}$$

The time-dependent states are linear superpositions of the spectroscopic energy eigenstates separated by the tunneling splitting, defined by the signed term difference between the two tunneling sublevels (eq 9):

$$\Delta\tilde{\nu}_T = \tilde{\nu}_{K_a}(\Gamma_{vt} = B^+) - \tilde{\nu}_{K_a}(\Gamma_{vt} = A^+) \tag{9}$$

3.2. Line Shape Analysis. The analysis of rovibrational line profiles can provide information about dynamic processes if various homogeneous and inhomogeneous contributions to the line profile can be determined separately. For $(HF)_2$ lines in the $N = 2$ polyad, two main contributions are expected: an inhomogeneous Gaussian contribution due to the Doppler effect, which is determined by the effective translational temperature of $(HF)_2$ and by the beam divergence with respect to the optical axis,[26,27] and a homogeneous Lorentzian contribution, which is related to the predissociation lifetime τ_{PD} of vibrationally excited $(HF)_2$. The exponential decay into the dissociation continuum (predissociation) with decay time τ_{PD} is related to the full width at half-maximum (fwhm) $\Delta\tilde{\nu}_{PD}$ (in cm^{-1}) or $\Delta\nu_{PD}$ (in Hz) of the Lorentzian line contribution by eq 10:

$$\tau_{PD} = 1/(2\pi c\Delta\tilde{\nu}_{PD}) = 1/(2\pi\Delta\nu_{PD}) \tag{10}$$

Contributions to the Lorentzian shape from collisions and spontaneous emission are negligible under our conditions. Because of the low rovibrational density of states,[51] broadening due to intramolecular vibrational redistribution (IVR) can also be excluded, although IVR coupling does exist and contributes to the mechanisms of vibrational predissociation. The convolution of both Gaussian and Lorentzian contributions will result in a Voigt line profile. By a nonlinear least-squares fit of experimental line profiles to a Voigt profile, the Gaussian and Lorentzian contributions can be obtained, in principle. Such a nonlinear fit, however, is, in practice, a very delicate matter, since the Gaussian width $\Delta\tilde{\nu}_G$ (fwhm) and the Lorentzian width $\Delta\tilde{\nu}_{PD}$ (fwhm) in the Voigt profile are highly correlated. In the presence of noise and finite resolution, they often cannot both be determined reliably, in particular, if one contribution dominates.[18,65] To assess the reliability of our determination of the Lorentzian width $\Delta\tilde{\nu}_{PD}$ (fwhm) from experimental line profiles, we first performed a test on synthetic Voigt profiles with known contributions and with noise and other conditions simulating the experiments.

Lines of the $N_j = 2_2$ band are simulated using a Lorentzian width $\Delta\nu_{PD}$ of 80 MHz and a Gaussian width $\Delta\nu_G$ of 160 MHz. The Voigt profile has a resolution of 15 MHz at 128 data points between −955 and +950 MHz around the origin. White Gaussian noise was added to the synthetic profile to obtain a signal-to-noise ratio of 50:1, which corresponds to typical experimental lines of the $K_a = 1 \leftarrow 0$ transition of the $N_j = 2_2$ band (see Figure 2, upper part). An unconstrained nonlinear least-squares fit of the synthetic Voigt line profile without noise results in exactly the predetermined line widths. With the added noise, an unconstrained fit of 10 lines differing by noise only yields $\Delta\nu_G = 155(7)$ MHz and $\Delta\nu_{PD} = 83(7)$ MHz, where the values in parentheses represent the standard deviation. Constraining the Gaussian width to the original value of 160 MHz, $\Delta\nu_{PD} = 79(2)$ MHz is obtained in the fit. It is thus clear that, if the Gaussian contribution is known from independent measurements, the Lorentzian contribution is determined much better in a constrained fit. For the experimental conditions applying to the 2_2 band, both contributions can be determined reliably. We draw attention, however, to the additional complication arising from the Doppler line shape in a supersonic beam expansion being not necessarily pure Gaussian. Under the present jet conditions, the Gaussian line shape was, however, found to be a good approximation for the HF monomer.[18] Also, for the N_2O overtone lines measured in the jet in parallel with the $(HF)_2$ lines, we found a pure Gaussian shape for the same low temperature. There is no appreciable high-temperature component from background gas at room temperature. It thus seems safe to also assume a pure Gaussian line shape for the Doppler component of the $(HF)_2$ lines.

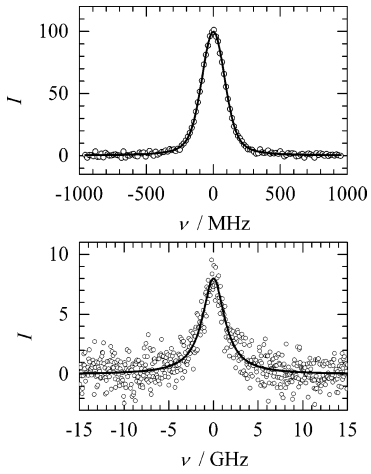

Figure 2. Synthetic Voigt line profiles (solid lines) with additional white noise (circles) simulating typical spectral lines obtained in the experiment for the $N_j = 2_1$ band (lower part) and the $N_j = 2_2$ band (upper part) of $(HF)_2$. *I* is the signal intensity in relative units; its maximum corresponds approximately to the absorbance $A/10^{-6}$ in the experimental CRD jet spectra. See text for details and further discussion.

To simulate lines of the $N_j = 2_1$ band, a Lorentzian width $\Delta\nu_{PD} = 3000$ MHz, a Gaussian width $\Delta\nu_G = 160$ MHz, and a signal-to-noise ratio of 8:1 were chosen, corresponding to typical experimental lines of the $K_a = 0 \leftarrow 0$ transition of the $N_j = 2_1$ band (see Figure 2, lower part). Six hundred data points between −14950 and +15000 MHz result in an effective resolution of 50 MHz. Again, the unconstrained Voigt fit of the synthetic line without noise recovers the original $\Delta\nu_{PD}$ and $\Delta\nu_G$, in spite of the low resolution. At the given noise level and with $\Delta\nu_G$ much smaller than $\Delta\nu_{PD}$, however, an unconstrained Voigt fit cannot determine the minor component $\Delta\nu_G$ at all: the fit of 10 lines with the added noise results in a Lorentzian line width $\Delta\nu_{PD} = 3110(150)$ MHz, but values of $\Delta\nu_G$ do not converge; they scatter within orders of magnitude. A constrained Voigt fit with $\Delta\nu_G$ fixed at 160 MHz yields $\Delta\nu_{PD} = 3145(85)$ MHz. A Lorentzian fit neglecting the Gaussian contribution yields

$\Delta\nu_{PD} = 3130(100)$ MHz. Under these conditions, it is thus adequate to use a Lorentzian fit instead of a Voigt fit for experimental lines of the $N_j = 2_1$ band to retrieve the Lorentzian contribution $\Delta\nu_{PD}$, which contains the relevant information about the predissociation lifetime. All the data reported below for $(HF)_2$ are from fits to "single spectra", which are obtained from many fixed frequency measurements averaging over the ring-down times at every single frequency. The uncertainties reported for such fits do not take into account uncertainties arising from changes in repeated, separated scans, and we will return to this point below.

3.3. Comparison with Theoretical Calculations. Quantum chemistry can be a powerful tool, in conjunction with high-resolution spectroscopy.[29,30,66,67] Calculations on potential energy surfaces (PESs) can predict the spectral region where a transition is found, aid the assignment of experimental spectra, and help to extract the molecular Hamiltonian. For the calculations[68] related to the present work, the PES used is the "SO-3", a semiempirical overtone-adjusted surface.[36,37] It is the currently most accurate in a long series of PESs of $(HF)_2$.[29] The method used to conduct 6D variational calculations on this surface is described by Bačić, Zhang, and co-workers.[41,69−72] A sequential diagonalization/truncation scheme together with a discrete variable representation (DVR) of the intermolecular stretching coordinate is employed to calculate rovibrational energy levels as developed by Bačić and Light[70−72] (see also related work on H_2O_2 and other molecules).[73−76]

In order to define the level of the theory compared to experiment, here we provide a brief description. Jacobi coordinates (r_1, r_2, R, θ_1, θ_2, τ) in the body-fixed (BF) frame are chosen to describe the internal motion of the HF dimer. r_1 and r_2 are the intramolecular vibrational coordinates of the monomers, R is the center of mass distance between the two monomers, θ_1 and θ_2 are the in-plane angles, and τ is the out-of-plane torsional angle. The 6D diatom−diatom rovibrational Hamiltonian for a total angular momentum J is thus given in the BF frame in Jacobi coordinates.

The sequential diagonalization/truncation scheme is applied to this 6D Hamiltonian. At each of the n equidistant DVR points R_m ($m = 1, 2, \ldots n$) along the intermolecular coordinate R, a matrix representation of $\hat{H}^{ad}(R_m)$ is constructed in the product basis of BF total angular momentum eigenfunctions and monomer vibrational eigenfunctions. The resulting set of eigenvectors depends parametrically on R and constitutes a 5D quasiadiabatic basis in r_1, r_2, θ_1, θ_2 and τ, which is well adapted to the PES. Consequently, for the construction of the matrix representation of the full (6D) Hamiltonian in the product basis of the 5D adiabatic eigenvectors and the basis functions in R, the number of 5D basis functions can be reduced significantly. Just 5D eigenvectors are retained, whose eigenvalues are below a certain energy cutoff criterion, determined by the maximum rovibrational level energies of interest. For two identical monomers, the Hamiltonian $\hat{H}$ is invariant with respect to the interchange of the two monomers. This permits the use of symmetry-adapted basis functions, which reduces the dimension of the Hamiltonian matrix. A more detailed description and discussion can be found in refs 41 and 68 and in the references cited therein. The eigenvalues thus calculated on the SO-3 6D potential hypersurface can be considered to be a very close approximation to the solution of the full 6D vibrational problem on that PES.

4. Results and Discussion

4.1. The 2_2 Sublevel. The sublevel $N_j = 2_2$ is the first component of the $N = 2$ polyad, for which an approximate rotational analysis was achieved[51] and which has been observed in a supersonic jet expansion thereafter.[18,77] To characterize the quality of the data achieved with the present experimental setup and to check upon comparison with the earlier results, we first investigated the $K_a = 1 \leftarrow 0$ perpendicular band of the $N_j = 2_2$ component of $(HF)_2$ near 7710 cm^{-1}. In Figure 3 the experimental spectrum (lower part) with the Q-branch region of this band is shown in comparison with a simulation (upper part). On top of the simulation, the rotational assignment is given. In this spectral region, mainly Q-branch transitions and some R-branch transitions are apparent. Both branches exhibit a distinct tunneling splitting. Maximum absorbances of about $A_{pp} = 1 \times 10^{-4}$ are observed under the present experimental jet conditions. For the Q-branch transitions of the lower tunneling state ($\Gamma_{vt} = A^+$), the intensity alternation for even and odd J-values due to the different nuclear spin statistical weights is clearly visible and thus establishes the symmetry assignment. Rotational parameters for the $K_a = 1$ level of the $N_j = 2_2$ component have been determined by a least-squares fit of the experimental spectrum to eq 7, and the spectroscopic constants obtained are summarized in Table 1. The band center is found to be at 7711.37956(66) cm^{-1}, in good agreement with previous results of 7711.8 cm^{-1} (ref 51), 7711.37914(7) cm^{-1} (ref 18), and 7711.3805(2) cm^{-1} (ref 77, which used a slightly different frequency calibration, superseded by the calibration given in ref 18) (values in parentheses represent one standard deviation in the units of the last figure quoted). The tunneling splitting for this band is $\Delta\tilde{\nu}_T = 0.0936(10)$ cm^{-1}, which is also in agreement with the previous results of 0.09406(10) cm^{-1} (ref 18) and 0.0942(3) cm^{-1} (ref 77). The simulation of the experimental relative intensities for $(HF)_2$ in the jet expansion

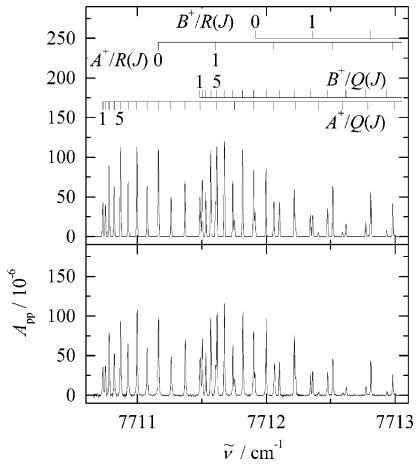

Figure 3. Q-branch region of the $K_a = 1 \leftarrow 0$ transition of the $N_j = 2_2$ band of $(HF)_2$. Lower part: experimental CRD spectrum in the slit jet expansion. Upper part: simulation for a rotational temperature of 25.9 K and assignment. A^+ or B^+ denote rotational branches terminating in the $\Gamma_{vt} = A^+$ or B^+ tunneling sublevel of the vibrationally excited state, respectively.

TABLE 1: Spectroscopic Parameters of the $K_a = 1$ Level of the $N_j = 2_2$ Band of $(HF)_2$

parameter	$\Gamma_{vt} = A^{+a}$	$\Gamma_{vt} = B^{+a}$
$\tilde{\nu}_1/cm^{-1}$	7711.37956(66)	7711.47319(66)
$\Delta\tilde{\nu}_T/cm^{-1}$	0.0936(10)	
B_1/cm^{-1}	0.220640(65)	0.22057 (37)
$D_1/10^{-6}$ cm^{-1}	2.39(16)	2.09(25)
$b_1/10^{-3}$ cm^{-1}	3.49(21)	3.7(14)
$N_{data} = 27$	$d_{rms} = 1.0 \times 10^{-3} cm^{-1}$	

[a] Values in parentheses represent one standard deviation in the units of the last figure quoted.

yields a rotational temperature of 25.9(4) K. The simulation is in excellent agreement with the experimental spectrum (see Figure 3), which finally corroborates the assignment and the spectroscopic constants obtained, as well as the effective rotational temperature.

To obtain the predissociation line width from the Lorentzian contribution in the Voigt profile, an unconstrained Voigt profile fit to all rotational lines was performed first. In an unconstrained fit, both Gaussian and Lorentzian contributions are allowed to vary, but they are highly correlated. The fit yields an averaged value of 167(10) MHz (fwhm) for the major Gaussian contribution, but a rather large scatter for the minor Lorentzian contribution. In a second step, the Gaussian contribution was thus kept fixed at 167 MHz in a constrained Voigt profile fit. An averaged predissociation line width (fwhm) of 121(12) MHz for the $\Gamma_{vt} = A^+$ tunneling sublevel and 84(11) MHz for $\Gamma_{vt} = B^+$ is then finally obtained. These values are again in agreement with previous results in the range 120 ± 7 MHz (ref 18), 114(11) MHz (ref 77) for $\Gamma_{vt} = A^+$ and 92 ± 10 MHz (ref 18) and 67(8) MHz for $\Gamma_{vt} = B^+$ (ref 77). As we have discussed above, the accuracy of the line width determinations should not be overstated, and the differences between the various experimental results are not significant, as the values obtained for the Lorentzian contributions also depend somewhat on uncertainties in the Doppler line shapes, which are not necessarily pure Gaussian (see also ref 18). The present results indicate a predissociation lifetime $\tau = 1.3(2)$ ns for $\Gamma_{vt} = A^+$ and $\tau = 1.9(3)$ ns for $\Gamma_{vt} = B^+$ in the $K_a = 1$, $N_j = 2_2$ state of $(HF)_2$. Because these parameters are obtained from lines in the same spectrum, some systematic effects cancel, and the difference can be considered marginally significant. For the HF monomer or N_2O transitions (see below), no significant Lorentzian contribution is expected. Under identical experimental jet conditions, they have a Gaussian line profile that agrees with the temperature from the Gaussian contribution determined for $(HF)_2$. The Gaussian line width 167(10) MHz (fwhm) corresponds to a formal translational temperature of 44.8(43) K for $(HF)_2$ (see also ref 18).

4.2. The 2_1 Sublevel. Without jet-cooling, many transitions are apparent in the spectral region of the $N = 2$ polyad of $(HF)_2$, most of them presumably arising from higher K_a levels of the ground state. However, only a few of these transitions could previously be reliably assigned to the $N_j = 2_2$ polyad component.[18,51,78] Other subbands clearly belong to the 2_1 sublevel.[51] Structures found between about 7525 and 7555 cm^{-1} in FTIR overtone spectra were tentatively attributed to the $N_j = 2_1$ component without any rotational assignment, and its band center was then very roughly estimated to be 7557 ± 15 cm^{-1}.[49,51] Only very rough estimates of the much larger line widths in 2_1 could previously be given.[18,51] In the region from 7543 to 7561 cm^{-1}, we indeed find evidence for the $K_a = 0 \leftarrow 0$ parallel transition of the $N_j = 2_1$ component of $(HF)_2$ in our experimental jet spectra. Two tunneling-split subbands are clearly apparent in the rotationally resolved *P*- and *R*-branches. In Figure 4 the experimental spectrum (lower part) is shown together with a simulation (upper part) and the rotational assignment (on top). The simulation was carried out for a rotational temperature of 26.0(10) K under these conditions and a Lorentzian line width (fwhm) of 3 GHz. The simulation and the experimental spectrum are in good agreement. There are a few additional lines, which have not been assigned to $N_j = 2_1$: narrow N_2O lines (some marked by plus signs in Figure 4) as well as three additional broad lines (marked by asterisks in Figure 4), which may belong to the $K_a = 1 \leftarrow 1$ transition of

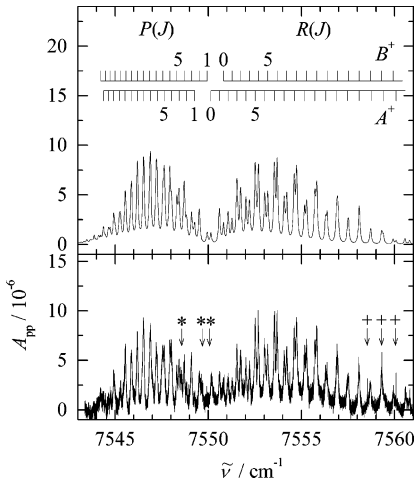

Figure 4. $K_a = 0 \leftarrow 0$ transition of the $N_j = 2_1$ band of $(HF)_2$. Lower part: experimental CRD spectrum in the slit jet expansion. Additional broad transitions, which are not due to that vibrational band, are marked with an asterisk; narrow transitions due to N_2O are marked with a plus sign. Upper part: simulation for a rotational temperature of 26.0 K and assignment (see also Figure 3).

the $N_j = 2_1$ polyad of $(HF)_2$ or possibly to N_2O-HF or Ar−HF clusters. The narrow lines are unambiguously assigned to N_2O overtone transitions by comparison with the literature line positions.[23,79] Compared to the $K_a = 1 \leftarrow 0$ transition of the $N_j = 2_2$ component, the integrated relative band strength of the $K_a = 0 \leftarrow 0$ transition of the $N_j = 2_1$ component is about two times larger, as estimated from approximate simulations of the bands under similar conditions. As the lines are much broader in $N_j = 2_1$, though, peak absorbances A_{app} are only about 1×10^{-5} under the present experimental jet conditions (see Figure 4), which is 1 order of magnitude smaller than that for the $N_j = 2_2$ component. Although the transitions are thus very weak, the experimental spectrum still has a signal-to-noise ratio of about 10:1 and is of sufficient quality for a detailed analysis and assignment.

We determined the rotational parameters for the $K_a = 0$ level of the $N_j = 2_1$ component by a least-squares fit of the experimental spectrum to eq 7. The peak positions from the jet spectrum and the rotational assignment of 56 lines are listed in Table 2, in addition to a comparison with calculated line positions. There are only a few instances with significant differences, perhaps indicative of local perturbations. In Table 3 the spectroscopic constants derived for the $K_a = 0$ level of the $N_j = 2_1$ component are given. The band center at 7550.3555(26) cm^{-1} and the tunneling splitting $\Delta\tilde{\nu}_T = 0.0150(37)$ cm^{-1} could be well determined. The values are in reasonable agreement with our ab initio calculations on the SO-3 potential energy hypersurface,[68] which yield a band center at 7543.3 cm^{-1} and a tunneling splitting of 0.009 cm^{-1}. Calculations on the SQSBDE potential energy hypersurface,[29,32] a commonly used predecessor of the SO-3, result in a band center at 7642.5 cm^{-1} and a tunneling splitting of 0.053 cm^{-1}.[69] The SO-3 surface clearly provides a significant improvement over SQSBDE. The higher-order constants D_0 and H_0 should be considered as effective values in Table 3, as they might include effects from other parameters not varied in the fit.

On the basis of the present determination of the $K_a = 0 \leftarrow 0$ band center, the perpendicular $K_a = 1 \leftarrow 0$ transition of the $N_j = 2_1$ component would be expected around 7580 cm^{-1} if one assumes an effective rotational constant A_{eff} between 35.4 cm^{-1} (the ground-state value)[61] and 26.4 cm^{-1} (the value for $N = 3$)[80] or any similar value.[18,51,77] For the $N_j = 2_2$ component, for

TABLE 2: Experimentally Observed and Calculated Line Positions $\tilde{\nu}$ of the $N_j = 2_1$ Band, with Assignment and with Experimentally Determined Predissociation Line Widths $\Delta\tilde{\nu}_{PD}$ (fwhm) from a Fit to a Lorentzian Profile

Γ_{vtr}[a]	Γ_r[a]	Γ_{vt}[a]	J_{K_a,K_c}[b]	←	Γ_{vtr}[a]	Γ_r[a]	Γ_{vt}[a]	g_k[c]	J_{K_a,K_c}[b]	o − c[d]	$\tilde{\nu}_{obs}/cm^{-1}$[e]	$\Delta\tilde{\nu}_{PD}/cm^{-1}$[e]
					P-Branch of the $K_a = 0 \leftarrow 0$ Transition							
A^-	B^-	B^+	$17_{0,17}$	←	A^+	A^+	A^+	10	$18_{0,18}$	−65	7544.2252(20)	
A^+	A^+	A^+	$14_{0,14}$	←	A^-	B^-	B^+	10	$15_{0,15}$	−17	7544.3630(22)	
B^+	A^+	B^+	$16_{0,16}$	←	B^-	B^-	A^+	6	$17_{0,17}$	−38	7544.4693(16)	
B^-	B^-	A^+	$13_{0,13}$	←	B^+	A^+	B^+	6	$14_{0,14}$	61	7544.6436(29)	
A^-	B^-	B^+	$15_{0,15}$	←	A^+	A^+	A^+	10	$16_{0,16}$	158	7544.7447(16)	
A^+	A^+	A^+	$12_{0,12}$	←	A^-	B^-	B^+	10	$13_{0,13}$	30	7544.9277(23)	
B^+	A^+	B^+	$14_{0,14}$	←	B^-	B^-	A^+	6	$15_{0,15}$	−148	7544.9830(56)	
A^+	A^+	A^+	$10_{0,10}$	←	A^-	B^-	B^+	10	$11_{0,11}$	3	7545.5377(98)	
B^+	A^+	B^+	$12_{0,12}$	←	B^-	B^-	A^+	6	$13_{0,13}$	−69	7545.5661(80)	
A^-	B^-	B^+	$7_{0,7}$	←	A^+	A^+	A^+	10	$8_{0,8}$	12	7547.2052(12)	
B^-	B^-	A^+	$5_{0,5}$	←	B^+	A^+	B^+	6	$6_{0,6}$	−5	7547.2642(16)	
B^+	A^+	B^+	$6_{0,6}$	←	B^-	B^-	A^+	6	$7_{0,7}$	−174	7547.5449(13)	
A^+	A^+	A^+	$4_{0,4}$	←	A^-	B^-	B^+	10	$5_{0,5}$	−17	7547.6408(7)	
A^-	B^-	B^+	$5_{0,5}$	←	A^+	A^+	A^+	10	$6_{0,6}$	29	7547.9343(7)	0.0901(21)
B^-	B^-	A^+	$3_{0,3}$	←	B^+	A^+	B^+	6	$4_{0,4}$	−58	7548.0254(8)	0.1004(21)
B^+	A^+	B^+	$4_{0,4}$	←	B^-	B^-	A^+	6	$5_{0,5}$	−21	7548.3088(8)	0.0910(28)
A^+	A^+	A^+	$2_{0,2}$	←	A^-	B^-	B^+	10	$3_{0,3}$	12	7548.4321(7)	0.0847(30)
A^-	B^-	B^+	$3_{0,3}$	←	A^+	A^+	A^+	10	$4_{0,4}$	10	7548.7024(6)	0.0874(22)
B^-	B^-	A^+	$1_{0,1}$	←	B^+	A^+	B^+	6	$2_{0,2}$	46	7548.8463(17)	0.1038(62)
B^+	A^+	B^+	$2_{0,2}$	←	B^-	B^-	A^+	6	$3_{0,3}$	−101	7549.0924(5)	0.0988(29)
A^+	A^+	A^+	$0_{0,0}$	←	A^-	B^-	B^+	10	$1_{0,1}$	−16	7549.2620(20)	0.107(18)
A^-	B^-	B^+	$1_{0,1}$	←	A^+	A^+	A^+	10	$2_{0,2}$	31	7549.5176(11)	0.0822(45)
B^+	A^+	B^+	$0_{0,0}$	←	B^-	B^-	A^+	6	$1_{0,1}$	−60	7549.9310(41)	
					R-Branch of the $K_a = 0 \leftarrow 0$ Transition							
B^-	B^-	A^+	$1_{0,1}$	←	B^+	A^+	B^+	6	$0_{0,0}$	96	7550.1507(45)	
A^+	A^+	A^+	$2_{0,2}$	←	A^-	B^-	B^+	10	$1_{0,1}$	47	7550.6011(10)	0.1144(46)
A^-	B^-	B^+	$1_{0,1}$	←	A^+	A^+	A^+	10	$0_{0,0}$	−1	7550.8145(17)	0.1340(71)
B^-	B^-	A^+	$3_{0,3}$	←	B^+	A^+	B^+	6	$2_{0,2}$	−16	7551.0609(13)	0.0968(50)
B^+	A^+	B^+	$2_{0,2}$	←	B^-	B^-	A^+	6	$1_{0,1}$	150	7551.2844(14)	0.1344(68)
A^+	A^+	A^+	$4_{0,4}$	←	A^-	B^-	B^+	10	$3_{0,3}$	−34	7551.5359(6)	0.0925(21)
A^-	B^-	B^+	$3_{0,3}$	←	A^+	A^+	A^+	10	$2_{0,2}$	39	7551.7386(8)	0.1175(28)
B^-	B^-	A^+	$5_{0,5}$	←	B^+	A^+	B^+	6	$4_{0,4}$	−39	7552.0227(11)	0.1278(42)
B^+	A^+	B^+	$4_{0,4}$	←	B^-	B^-	A^+	6	$3_{0,3}$	91	7552.2194(10)	0.0799(34)
A^+	A^+	A^+	$6_{0,6}$	←	A^-	B^-	B^+	10	$5_{0,5}$	−55	7552.5186(6)	0.1053(19)
A^-	B^-	B^+	$5_{0,5}$	←	A^+	A^+	A^+	10	$4_{0,4}$	−25	7552.6936(6)	0.1065(21)
B^-	B^-	A^+	$7_{0,7}$	←	B^+	A^+	B^+	6	$6_{0,6}$	−36	7553.0282(7)	0.0989(31)
B^+	A^+	B^+	$6_{0,6}$	←	B^-	B^-	A^+	6	$5_{0,5}$	−28	7553.1894(7)	0.1004(33)
A^+	A^+	A^+	$8_{0,8}$	←	A^-	B^-	B^+	10	$7_{0,7}$	−28	7553.5465(7)	0.1016(25)
A^-	B^-	B^+	$7_{0,7}$	←	A^+	A^+	A^+	10	$6_{0,6}$	−14	7553.6968(7)	0.1092(24)
B^-	B^-	A^+	$9_{0,9}$	←	B^+	A^+	B^+	6	$8_{0,8}$	20	7554.0789(8)	0.1083(44)
B^+	A^+	B^+	$8_{0,8}$	←	B^-	B^-	A^+	6	$7_{0,7}$	24	7554.2166(7)	0.1198(37)
A^+	A^+	A^+	$10_{0,10}$	←	A^-	B^-	B^+	10	$9_{0,9}$	9	7554.6153(6)	0.0980(27)
A^-	B^-	B^+	$9_{0,9}$	←	A^+	A^+	A^+	10	$8_{0,8}$	7	7554.7406(6)	0.1286(29)
B^-	B^-	A^+	$11_{0,11}$	←	B^+	A^+	B^+	6	$10_{0,10}$	57	7555.1680(10)	0.1199(55)
B^+	A^+	B^+	$10_{0,10}$	←	B^-	B^-	A^+	6	$9_{0,9}$	−13	7555.2740(8)	0.1454(46)
A^+	A^+	A^+	$12_{0,12}$	←	A^-	B^-	B^+	10	$11_{0,11}$	12	7555.7224(8)	0.1134(67)
A^-	B^-	B^+	$11_{0,11}$	←	A^+	A^+	A^+	10	$10_{0,10}$	5	7555.8211(7)	0.1480(59)
B^-	B^-	A^+	$13_{0,13}$	←	B^+	A^+	B^+	6	$12_{0,12}$	14	7556.2934(23)	
B^+	A^+	B^+	$12_{0,12}$	←	B^-	B^-	A^+	6	$11_{0,11}$	15	7556.3771(22)	
A^+	A^+	A^+	$14_{0,14}$	←	A^-	B^-	B^+	10	$13_{0,13}$	17	7556.8776(19)	0.0873(51)
A^-	B^-	B^+	$13_{0,13}$	←	A^+	A^+	A^+	10	$12_{0,12}$	96	7556.9504(14)	0.0718(40)
B^-	B^-	A^+	$15_{0,15}$	←	B^+	A^+	B^+	6	$14_{0,14}$	−126	7557.4620(11)	
B^+	A^+	B^+	$14_{0,14}$	←	B^-	B^-	A^+	6	$13_{0,13}$	102	7557.5267(39)	
B^+	A^+	B^+	$18_{0,18}$	←	B^-	B^-	A^+	6	$17_{0,17}$	−106	7559.9264(26)	0.106(13)
B^-	B^-	A^+	$19_{0,19}$	←	B^+	A^+	B^+	6	$18_{0,18}$	34	7560.078(14)	
A^-	B^-	B^+	$19_{0,19}$	←	A^+	A^+	A^+	10	$18_{0,18}$	86	7560.5857(15)	
A^+	A^+	A^+	$20_{0,20}$	←	A^-	B^-	B^+	10	$19_{0,19}$	−11	7560.7949(27)	

[a] Γ_r is the rotational species, Γ_{vt} is the tunneling-vibrational species, and $\Gamma_{vtr} = \Gamma_{vt}\Gamma_r$ is the total symmetry species. [b] J, K_a, and K_c are the rotational quantum numbers. [c] g_k is the spin statistical weight. [d] "o − c" is the difference between the observed and calculated position in 10^{-4} cm^{-1}. [e] Values in parentheses represent one standard deviation in the units of the last figure quoted.

example, $A_{eff} = 28.6$ cm^{-1}.[18,51,77] Our jet measurements in the region around 7580 cm^{-1} did not reveal any absorption features that could be assigned to this subband. This is not too surprising, however, since the $N_j = 2_1$ band has dominantly parallel character, with only very weak perpendicular transitions. Apparently, the perpendicular $K_a = 1 \leftarrow 0$ transition of the $N_j = 2_1$ component is too weak to be observed under the present experimental conditions.

4.3. Predissociation Line Widths in the 2_1 Sublevel. The line widths observed in the jet spectrum of the $N_j = 2_1$ component are, with about 3 GHz (fwhm), very broad, much broader than those in the $N_j = 2_2$ component. The rovibrational line profiles are very well reproduced by a Lorentzian profile (see Figure 5), since the Gaussian contribution (167 MHz fwhm, see above) is negligible compared to the total line width. The large Lorentzian contribution is due to fast predissociation. In

TABLE 3: Spectroscopic Parameters of the $K_a = 0$ Level of the $N_j = 2_1$ Band of $(HF)_2$

parameter	$\Gamma_{vt} = A^{+a}$	$\Gamma_{vt} = B^{+a}$
$\tilde{\nu}_0/cm^{-1}$	7550.3555(26)	7550.3705(26)
$\Delta\tilde{\nu}_T/cm^{-1}$	0.0150(37)	
B_0/cm^{-1}	0.222144(92)	0.222064 (91)
$D_0/10^{-6}\ cm^{-1}$	4.41(65)	3.19(65)
$H_0/10^{-12}\ cm^{-1}$	7800(1100)	2800(1200)
$N_{data} = 56$	$d_{rms} = 6.4 \times 10^{-3} cm^{-1}$	

[a] Values in parentheses represent one standard deviation in the units of the last figure quoted.

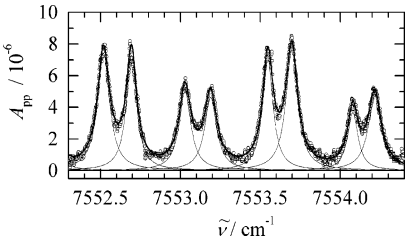

Figure 5. Detail of the *R*-branch of the $K_a = 0 \leftarrow 0$ transition of the $N_j = 2_1$ band of $(HF)_2$ observed by CRD spectroscopy in a slit jet expansion. The solid lines are Lorentzian lines with 0.1 cm^{-1} fwhm obtained by a fit to the experimental spectrum; the bold line is the sum of the individual Lorentzian contributions.

TABLE 4: Average Values of the Predissociation Line Widths (fwhm) of the $K_a = 0 \leftarrow 0$ Transition of $N_j = 2_1$ for the *P* and *R* Branch and the Two Tunneling States

	Γ_{vt}	$\Delta\nu_{PD}$/GHz[a]
P-branch	A^+	2.97(30)
	B^+	2.70(18)
R-branch	A^+	3.16(36)
	B^+	3.47(70)

[a] Values in parentheses represent one standard deviation in the units of the last figure quoted. Differences between branches and sublevels are thus not significant.

order to obtain the predissociation widths $\Delta\nu_{PD}$, rovibrational lines from the jet spectrum were simulated using a Lorentzian profile. This approximation is expected to introduce only a small error into the determination of $\Delta\nu_{PD}$, smaller than the standard deviation of the $\Delta\nu_{PD}$ determined from the fit. In Table 2, the widths of 34 selected lines are listed. Other lines are less suitable for a reliable determination of Δn_{PD}, since they are overlapped.

Averaged predissociation line widths of the different A^+ and B^+ tunneling states obtained from *P*- and *R*-branch transitions, respectively, are summarized in Table 4. Within two standard deviations, there is no significant difference apparent for the widths obtained from the two branches and symmetry species. We therefore quote as an averaged predissociation line width $\Delta\nu_{PD} = 3.19(55)$ GHz for this $K_a = 0$, $N_j = 2_1$ state with a resulting predissociation lifetime $\tau = 49.9(84)$ ps, which is much shorter than the corresponding lifetime in the $K_a = 1$, $N_j = 2_2$ state of $(HF)_2$ (1.6 ns). The vibrational excitation in the hydrogen-bond donor HF in $N_j = 2_1$ therefore greatly enhances predissociation, in agreement with intuition (see below). We should also note that the individual line fits reported in Table 2 give uncertainties of line width parameters as they result from fits to single lines (which contain many measured points). The uncertainties thus express, in essence, the consistency of the data points in one line to provide the parameters indicated. They do not express the result of an uncertainty estimate, as might be obtained from several independent experiments for the same level.[58] Such an estimate is possible for a number of lines, which correspond to the same upper level, thus having the same physical level parameters such as width or level position. From these cases in Table 2, one sees that the real uncertainties are much larger than suggested by the individual line fit parameters. This is in agreement with the discussion in ref 18. One might make a combined fit of data for levels including level positions and widths, as we often do just for precise term value determinations in high-resolution, line-resolved spectroscopy.[81] We have not done this for the present data because, at most, two independent data sets were obtained for a given level, and often only one.

5. Conclusions

The application of high-resolution cw-CRD spectroscopy enabled us to present the first rotationally resolved spectrum, including full assignment, of the $N_j = 2_1$ component of $(HF)_2$ in a supersonic jet expansion. Spectroscopic constants, the experimental band center, and tunneling splitting have been obtained; the values are in reasonable agreement with ab initio calculations. The results of the reinvestigation of the $K_a = 1 \leftarrow 0$ transition of $N_j = 2_2$ are in agreement with previous work.[18,51,77] The new results on 2_1 provide important new information. Our parallel measurement of 2_1 and 2_2 provides an estimate of the relative integrated intensities, which are rather similar for both bands, in agreement with matrix studies[82,83] and our early estimates.[51]

The analysis of the spectra provides insight into the dynamic processes involving the hydrogen bond in $(HF)_2$. Vibrational predissociation is distinctly vibrational-mode specific; it depends strongly on the excited local mode(s) and the number of stretching quanta. Vibrational excitation of the hydrogen-bond donor mode (the hydrogen-bonded monomer) results in much shorter lifetimes (about 50 ps) than excitation of the hydrogen-bond acceptor mode (the free monomer) (about 1.6 ns). This behavior can be understood qualitatively by considering the equilibrium structure of the HF dimer (Figure 1). The H−F bond of the hydrogen-bonded monomer is nearly in-line with the hydrogen bond between the monomer units of the dimer. A stretching excitation of the hydrogen-bonded monomer will strongly affect the hydrogen atom involved in the hydrogen bond and thus strongly influence the bond dissociation. The H−F bond of the free monomer on the other hand is about 65° off the axis of the hydrogen bond and not directly involved in hydrogen bonding. The fluorine atom, which is involved in the hydrogen bond, will not be affected much by an excitation of the HF stretching mode, which explains the smaller effect of HF stretching excitation within the free monomer unit compared to the hydrogen-bonded monomer unit. A K_a-dependence is observed, but does not occur uniformly in all modes. There is also a small, barely significant dependence of the lifetime on the nuclear spin symmetry, resulting in longer lifetimes for the upper state ($\Gamma_{vt} = B^+$) compared to the lower ($\Gamma_{vt} = A^+$) state. The highly nonstatistical, mode-selective nature of vibrational predissociation at energies of 7500−7800 (*hc*) cm^{-1}, exceeding the hydrogen bond dissociation energy by more than 7 times the value of $D_0 \simeq 1060$ (*hc*) cm^{-1} is in qualitative agreement with earlier results,[18,51] but now is precisely and quantitatively established.

Mode-selective dynamics is also found for the second process with an even lower barrier for reaction: the hydrogen-bond switching with a barrier along the reaction path of about 350 (*hc*) cm^{-1} (ref 37). In the ground state, the hydrogen-bond switching process in $(HF)_2$ is a tunneling motion, where the two monomer subunits of the dimer exchange their respective roles in the hydrogen bond. The hydrogen-bonded monomer

TABLE 5: Experimental and Calculated Tunneling Splittings $\Delta\nu_T = c\cdot\Delta\tilde{\nu}_T$ (Eq 9) for Several Vibrational States of $(HF)_2$. Variational Calculations Were Carried out Using the SO-3 Potential Energy Hypersurface of $(HF)_2$[a]

	$\Delta\nu_T$/GHz		
	$K_a = 0$		$K_a = 1$
N_j	exptl[b]	6D calcd[c,d]	exptl[b]
0	19.76070(2)[e,f,g,h]	17.70	31.933132(9)[f,g]
1_1	6.998(12)[i]	5.08	10.225(27)[i]
1_2	−6.4618(81)[i]	−5.44	−10.4888(27)[i]
2_1	0.45(11)[j]	0.27	
2_2	6 ± 1[k]	6.21	2.85[l]
2_2	6.344(8)[m]	6.21	2.82(1)[m]
2_2	6.357(15)[n]	6.21	2.8260(90)[n]
2_2	6.468[o]	6.21	2.808(30)[j]
2_3	20.283[o]	14.20	28.476[o]
3_1	<3[p]	−0.90[c]	
3_2	0.072(18)[p]	<0.15[c]	<0.16[p]
3_4	−11.63(6)[p]	−9.30[c]	

[a] States are characterized by the polyad quantum number N_j and the K_a quantum number. [b] Values in parentheses represent one standard deviation in the units of the last figure quoted. [c] Reference 41. [d] Reference 68. [e] Reference 4. [f] Reference 42. [g] Reference 61. [h] Reference 85. [i] Reference 48. [j] This work. [k] Reference 51. [l] Reference 78. [m] Reference 18. [n] Reference 77. [o] Reference 95. [p] Reference 96.

(donor) becomes the free monomer (acceptor), and vice versa (see Figure 1). A list of tunneling splittings $\Delta\tilde{\nu}_T$ for the ground state $N = 0$ and the polyads $N = 1-3$ of $(HF)_2$ is given in Table 5. Experimental values for $K_a = 0$ and 1 available from the literature or from the present investigation are presented together with calculated values for the $K_a = 0$ state. The 6D variational calculations[68] were carried out on the SO-3 potential energy hypersurface of $(HF)_2$ and agree reasonably well with experimental tunneling splittings concerning the magnitude and sign of the tunneling splitting (as defined in eq 2). The sign determines the symmetry ordering of polyad levels. The sign of the tunneling splitting in the $N = 2$ polyad has been the subject of long-standing discussions,[69,84] which are now resolved by the present results in favor of an early tentative assignment[51] of 2_2. Vibrational HF-stretching excitation of just one local mode results in a pronounced decrease in the tunneling splitting and thus in an increase of the tunneling period for hydrogen-bond switching compared to the vibrational ground state. After simultaneous excitation of both local modes, however, a much less pronounced change is expected. A simple model may explain this finding qualitatively: in the hydrogen bond switching process, HF-stretching excitation has to be redistributed from one monomer unit to the other if only one local mode is excited. In this case, vibrational excitation inhibits the tunneling process. If both modes are excited, this redistribution of vibrational excitation has to occur to a lesser extent, and thus the tunneling splitting is closer to the ground-state value. Simple models like this have been suggested repeatedly to explain the sign and magnitude of tunneling splittings in the ground state and as a function of HF stretching excitation.[85−91] None of these, however, are able to provide a globally and quantitatively correct picture as do the calculations on the SO-3 surface.[68]

An interesting general property of the hydrogen bond switching process in $(HF)_2$ is its tunneling nature, although the process occurs at energy exceeding the "barrier" for the tunneling process by a factor of much more than 20 in the $N = 2$ polyad of $(HF)_2$. We thus can characterize the switching as mode-selective quasiadiabatic above barrier tunneling, very similar to stereomutation in H_2O_2[75,76] and ammonia isotopomers.[92−94] A new mechanism arises in $(HF)_2$ for vibrationally inhibiting above barrier tunneling: tunneling switching is inhibited by the necessary IVR between the local excitations.

In a subsequent paper, we also apply the new spectroscopic technique to observe the remaining component of the $N = 2$ polyad, the $N_j = 2_3$ component.[95] This will allow us to study mode-specific dynamics in the HF dimer in the $N = 2$ polyad more systematically, comparing all possible ways for distribution of vibrational HF-stretching excitation among both HF subunits. Our results obtained from jet-cooled spectra will also provide a key to assign and analyze transitions from higher K_a levels of the ground state, which are apparent in FTIR spectra at higher temperatures.

Acknowledgment. We are grateful to Hans Hollenstein for help and discussions. We also acknowledge discussions with Zlatko Bačić, Jochen Blumberger, Carine Manca, Holger Müller, Katharina von Puttkamer-Al Shamery, Ruth Signorell, and Martin Suhm. Our work is supported financially by the ETH Zürich and the Schweizerischer Nationalfonds.

References and Notes

(1) *Atomic and Molecular Beam Methods*; Scoles, G., Ed.; Oxford University Press: New York, 1988 and 1992; Vols. 1 and 2.
(2) Gough, T. E.; Miller, R. E.; Scoles, G. *Appl. Phys. Lett.* **1977**, *30*, 338.
(3) Lehmann, K. K.; Scoles, G.; Pate, B. H. *Annu. Rev. Phys. Chem.* **1994**, *45*, 241.
(4) Dyke, T. R.; Howard, B. J.; Klemperer, W. *J. Chem. Phys.* **1972**, *56*, 2442.
(5) Sinha, M. P.; Schultz, A.; Zare, R. N. *J. Chem. Phys.* **1973**, *58*, 549.
(6) Smalley, R. E.; Ramakrishna, B. L.; Levy, D. H.; Wharton, L. *J. Chem. Phys.* **1974**, *61*, 4363.
(7) Smalley, R. E.; Wharton, L.; Levy, D. H. *Acc. Chem. Res.* **1977**, *10*, 139.
(8) Levy, D. H. *Annu. Rev. Phys. Chem.* **1980**, *31*, 197.
(9) Dübal, H. R.; Quack, M.; Schmitt, U. *Chimia* **1984**, *38*, 438.
(10) Amrein, A.; Quack, M.; Schmitt, U. *J. Phys. Chem.* **1988**, *92*, 5455.
(11) Quack, M. *Annu. Rev. Phys. Chem.* **1990**, *41*, 839.
(12) Snels, M.; Quack, M. *J. Chem. Phys.* **1991**, *95*, 6355.
(13) Snels, M.; Beil, A.; Hollenstein, H.; Quack, M.; Schmitt, U.; D'Amato, F. *J. Chem. Phys.* **1995**, *103*, 8846.
(14) Beil, A.; Luckhaus, D.; Marquardt, R.; Quack, M. *Faraday Discuss.* **1994**, *99*, 49.
(15) Bauder, A.; Beil, A.; Luckhaus, D.; Müller, F.; Quack, M. *J. Chem. Phys.* **1997**, *106*, 7558.
(16) D'Amico, G. D.; Snels, M.; Hollenstein, H.; Quack, M. *Phys. Chem. Chem. Phys.* **2002**, *4*, 1531.
(17) Boudon, V.; Rotger, M.; He, Y.; Hollenstein, H.; Quack, M.; Schmitt, U. *J. Chem. Phys.* **2002**, *117*, 3196.
(18) He, Y.; Müller, H.; Quack, M.; Suhm, M. A. *Z. Phys. Chem.* **2007**, *221*, 1581.
(19) Albert, S.; Bauerecker, S.; Quack, M.; Steinlin, A. *Mol. Phys.* **2007**, *105*, 541.
(20) Scherer, J. J.; Paul, J. B.; O'Keefe, A.; Saykally, R. J. *Chem. Rev.* **1997**, *97*, 25.
(21) Romanini, D.; Lehmann, K. K. *J. Chem. Phys.* **1993**, *99*, 6287.
(22) Martin, J.; Paldus, B. A.; Zalicki, P.; Wahl, E. H.; Owano, T. G.; Harris, J. S., Jr.; Kruger, C. H.; Zare, R. N. *Chem. Phys. Lett.* **1996**, *258*, 63.
(23) He, Y. B.; Hippler, M.; Quack, M. *Chem. Phys. Lett.* **1998**, *289*, 527.
(24) Paldus, B. A.; Harb, C. C.; Spence, T. G.; Wilke, B.; Xie, J.; Harris, J. S.; Zare, R. N. *J. Appl. Phys.* **1998**, *83*, 3991.
(25) Romanini, D.; Kachanov, A. A.; Stoeckel, F. *Chem. Phys. Lett.* **1997**, *270*, 538.
(26) Hippler, M.; Quack, M. *Chem. Phys. Lett.* **1999**, *314*, 273.
(27) Hippler, M.; Quack, M. *J. Chem. Phys.* **2002**, *116*, 6045.
(28) Quack, M. *Chimia* **2003**, *57*, 147.
(29) Quack, M.; Suhm, M. A. Potential energy hypersurfaces for hydrogen bonded clusters $(HF)_n$. In *Conceptual Perspectives in Quantum Chemistry*; Kryachko, E. S., Calais, J. L., Eds.; Kluwer: Dordrecht, The Netherlands, 1997; p 415.
(30) Quack, M.; Suhm, M. A. Spectroscopy and quantum dynamics of hydrogen fluoride clusters. In *Advances in Molecular Vibrations and Collision Dynamics: Molecular Clusters*; Bacic, Z., Bowman, J., Eds.; JAI Press, Inc.: Stamford, CT, and London, England, 1998; Vol. 3, p 205.

(31) Yarkony, D. R.; O'Neil, S. V.; Schaefer, H. F., III; Baskin, C. P.; Bender, C. F. *J. Chem. Phys.* **1974**, *60*, 855.
(32) Quack, M.; Suhm, M. A. *J. Chem. Phys.* **1991**, *95*, 28.
(33) Kofranek, M.; Lischka, H.; Karpfen, A. *Chem. Phys.* **1988**, *121*, 137.
(34) Bunker, P. R.; Carrington, T.; Gomez, P. C.; Marshall, M. D.; Kofranek, M.; Lischka, H.; Karpfen, A. *J. Chem. Phys.* **1989**, *91*, 5154.
(35) Quack, M.; Suhm, M. A. *Mol. Phys.* **1990**, *69*, 791 (tables in supplementary publication deposited in the British Library unter No. SUP 16090).
(36) Klopper, W.; Quack, M.; Suhm, M. A. *Chem. Phys. Lett.* **1996**, *261*, 35.
(37) Klopper, W.; Quack, M.; Suhm, M. A. *J. Chem. Phys.* **1998**, *108*, 10096 (88 pages of supplementary material published as AIP Document No PAPS JCPS 16-108-303 820-88 by the American Institute of Physics, Physics Auxiliary Publication Service).
(38) Zhang, D. H.; Wu, Q.; Zhang, J. Z. H. *J. Chem. Phys.* **1995**, *102*, 124.
(39) Zhang, D. H.; Wu, Q.; Zhang, J. Z. H.; Vondirke, M.; Bacic, Z. *J. Chem. Phys.* **1995**, *102*, 2315.
(40) Necoechea, W. C.; Truhlar, D. G. *Chem. Phys. Lett.* **1996**, *248*, 182.
(41) Bacic, Z.; Qiu, Y.; Zhang, J. Z. H.; Müller, H. B.; Quack, M. To be submitted for publication.
(42) Quack, M.; Suhm, M. A. *Chem. Phys. Lett.* **1990**, *171*, 517.
(43) Sun, H.; Watts, R. O. *J. Chem. Phys.* **1990**, *92*, 603.
(44) Quack, M.; Suhm, M. A. *Chem. Phys. Lett.* **1995**, *234*, 71.
(45) von Puttkamer, K.; Quack, M. *Mol. Phys.* **1987**, *62*, 1047.
(46) von Puttkamer, K.; Quack, M.; Suhm, M. A. *Infrared Phys.* **1989**, *29*, 535.
(47) Pine, A. S.; Lafferty, W. J. *J. Chem. Phys.* **1983**, *78*, 2154.
(48) Pine, A. S.; Lafferty, W. J.; Howard, B. J. *J. Chem. Phys.* **1984**, *81*, 2939.
(49) von Puttkamer, K.; Quack, M. *Chimia* **1985**, *39*, 358.
(50) von Puttkamer, K.; Quack, M. *Faraday Discuss.* **1986**, 377.
(51) von Puttkamer, K.; Quack, M. *Chem. Phys.* **1989**, *139*, 31.
(52) Dayton, D. C.; Jucks, K. W.; Miller, R. E. *J. Chem. Phys.* **1989**, *90*, 2631.
(53) Oudejans, L.; Miller, R. E. *J. Chem. Phys.* **2000**, *113*, 971.
(54) Quack, M.; Stohner, J.; Suhm, M. A. *J. Mol. Struct.* **2001**, *599*, 381.
(55) Lovejoy, C. M.; Nesbitt, D. J. *Rev. Sci. Instrum.* **1987**, *58*, 807.
(56) Hollenstein, H.; Quack, M.; Richard, E. *Chem. Phys. Lett.* **1994**, *222*, 176.
(57) Toth, R. A. *Appl. Opt.* **1994**, *33*, 4851.
(58) Cohen, E. R.; Cvitas, T.; Frey, J. G.; Holmström, B.; Kuchitsu, K.; Marquardt, R.; Mills, I.; Pavese, F.; Quack, M.; Stohner, J.; Strauss, H. L.; Takami, M.; Thor, A. J. *Quantities, Units and Symbols in Physical Chemistry*, 3rd ed.; IUPAC, RSC Publishing: Cambridge, U.K., 2007.
(59) Lovejoy, C. M.; Nesbitt, D. J. *J. Chem. Phys.* **1989**, *90*, 4671.
(60) Quack, M. *Mol. Phys.* **1977**, *34*, 477.
(61) Quack, M.; Suhm, M. A. *Chem. Phys. Lett.* **1991**, *183*, 187.
(62) Herzberg, G. *Molecular Spectra and Molecular Structure: Infrared and Raman Spectra of Polyatomic Molecules*, 1st ed.; van Nostrand: New York, 1945; Vol. II.
(63) Hund, F. *Z. Phys.* **1926**, *40*, 742.
(64) Hund, F. *Z. Phys.* **1927**, *43*, 805.
(65) Di Rocco, H. O.; Iriarte, D. I.; Pomarico, J. *Appl. Spectrosc.* **2001**, *55*, 822.
(66) Yamaguchi, Y.; Schaefer, H. F., III; Osamura, Y.; Goddard, J. D. *A New Dimension in Quantum Chemistry: Analytical Derivative Methods in Ab Initio Molecular Electronic Structure Theory*; Oxford University Press: Oxford, 1994.
(67) Tschumper, G. S.; Leininger, M. L.; Hoffman, B. C.; Valeev, E. F.; Schaefer, H. F.; Quack, M. *J. Chem. Phys.* **2002**, *116*, 690.
(68) Blumberger, J.; Oeltjen, L.; Quack, M.; Bacic, Z.; Qiu, Y.; Zhang, J. Z. H. *Faraday Discuss.* **2001**, *118*, 431 (additional work to be submitted for publication).
(69) Wu, Q.; Zhang, D. H.; Zhang, J. Z. H. *J. Chem. Phys.* **1995**, *103*, 2548.
(70) Bacic, Z.; Light, J. C. *Annu. Rev. Phys. Chem.* **1989**, *40*, 469.
(71) Bacic, Z.; Light, J. C. *J. Chem. Phys.* **1986**, *85*, 4594.
(72) Bacic, Z.; Light, J. C. *J. Chem. Phys.* **1987**, *86*, 3065.
(73) Luckhaus, D.; Quack, M. *Chem. Phys. Lett.* **1992**, *190*, 581.
(74) Ha, T. K.; Luckhaus, D.; Quack, M. *Chem. Phys. Lett.* **1992**, *190*, 590.
(75) Fehrensen, B.; Luckhaus, D.; Quack, M. *Chem. Phys. Lett.* **1999**, *300*, 312.
(76) Fehrensen, B.; Luckhaus, D.; Quack, M. *Chem. Phys.* **2007**, *338*, 90.
(77) Suhm, M. A.; Farrell, J. T.; McIlroy, A.; Nesbitt, D. J. *J. Chem. Phys.* **1992**, *97*, 5341.
(78) Signorell, R.; He, Y.; Müller, H.; Quack, M.; Suhm, M. A. High resolution diode laser and FTIR spectroscopy of $(HF)_n$ and its isotopomers. In *Proceedings of the 10th Symposium on Atomic, Molecular, Cluster, Ion and Surface Physics, SASP 96*; Maier, J. P., Quack, M., Eds.; vdf Hochschulverlag Publishers: Zürich, Switzerland, 1996; p 256.
(79) Weirauch, G.; Kachanov, A. A.; Campargue, A.; Bach, M.; Herman, M.; Vander Auwera, J. *J. Mol. Spectrosc.* **2000**, *202*, 98.
(80) Chang, H. C.; Klemperer, W. *J. Chem. Phys.* **1993**, *98*, 9266.
(81) Ulenikov, O. N.; Bekhtereva, E. S.; Grebneva, S. V.; Hollenstein, H.; Quack, M. *Mol. Phys.* **2006**, *104*, 3371.
(82) Goubet, M.; Asselin, P.; Manceron, L.; Soulard, P.; Perchard, J. P. *Phys. Chem. Chem. Phys.* **2003**, *5*, 3591.
(83) Goubet, M.; Asselin, P.; Soulard, P.; Perchard, J. P. *Phys. Chem. Chem. Phys.* **2003**, *5*, 5365.
(84) Jensen, P.; Bunker, P. R.; Karpfen, A.; Kofranek, M.; Lischka, H. *J. Chem. Phys.* **1990**, *93*, 6266.
(85) Howard, B. J.; Dyke, T. R.; Klemperer, W. *J. Chem. Phys.* **1984**, *81*, 5417.
(86) Chang, H. C.; Klemperer, W. *J. Chem. Phys.* **1996**, *104*, 7830.
(87) Mills, I. M. *J. Phys. Chem.* **1984**, *88*, 532.
(88) Hougen, J. T.; Ohashi, N. *J. Mol. Spectrosc.* **1985**, *109*, 134.
(89) Fraser, G. T. *J. Chem. Phys.* **1989**, *90*, 2097.
(90) Sibert, E. L. *J. Phys. Chem.* **1989**, *93*, 5022.
(91) Hancock, G. C.; Truhlar, D. G. *J. Chem. Phys.* **1989**, *90*, 3498.
(92) Snels, M.; Hollenstein, H.; Quack, M. *J. Chem. Phys.* **2006**, *125*, 194319.
(93) Snels, M.; Hollenstein, H.; Quack, M. *J. Chem. Phys.* **2003**, *119*, 7893.
(94) Marquardt, R.; Quack, M.; Thanopulos, I.; Luckhaus, D. *J. Chem. Phys.* **2003**, *118*, 643.
(95) Hippler, M.; Oeltjen, L.; Quack, M. To be submitted for publication.
(96) Chang, H. C.; Klemperer, W. *J. Chem. Phys.* **1994**, *100*, 1.